

PCCP

Accepted Manuscript



This is an *Accepted Manuscript*, which has been through the Royal Society of Chemistry peer review process and has been accepted for publication.

Accepted Manuscripts are published online shortly after acceptance, before technical editing, formatting and proof reading. Using this free service, authors can make their results available to the community, in citable form, before we publish the edited article. We will replace this *Accepted Manuscript* with the edited and formatted *Advance Article* as soon as it is available.

You can find more information about *Accepted Manuscripts* in the [Information for Authors](#).

Please note that technical editing may introduce minor changes to the text and/or graphics, which may alter content. The journal's standard [Terms & Conditions](#) and the [Ethical guidelines](#) still apply. In no event shall the Royal Society of Chemistry be held responsible for any errors or omissions in this *Accepted Manuscript* or any consequences arising from the use of any information it contains.

Cite this: DOI: 10.1039/c0xx00000x

ARTICLE TYPE

www.rsc.org/xxxxxx

Anode modification with capacitive materials for a microbial fuel cell: an increase in transient power or stationary power

Chunhua Feng,*^a Zhisheng Lv,^a Xiaoshuang Yang^a and Chaohai Wei^a

Received (in XXX, XXX) Xth XXXXXXXXX 20XX, Accepted Xth XXXXXXXXX 20XX

DOI: 10.1039/b000000x

Extensive efforts have been devoted to improve the anode performance of a microbial fuel cell (MFC) by using modified carbon-based anode materials, but most of them did not recognize that the power performance measured by the commonly-used varying circuit resistance (VCR) or linear sweep voltammetry (LSV) method was overestimated due to the effect of anode capacitance. Here, we examined and compared the transient power and the stationary power of a series of MFCs equipped with the polypyrrole/graphene oxide (PPy/GO)-modified graphite felt anodes. It was found that noticeable transient power was recorded when the VCR or LSV method was chosen for power measurement. Calculations on the contribution of different sources to the measured maximum power density showed that the discharge of bio-electrons stored in the high-capacitance anode was a dominant contributor, especially when the time duration (for the VCR method) was not sufficiently long or the scan rate (for the LSV method) was not sufficiently low. Although anode modification with capacitive materials can result in the increased stationary power obtained from the fed-batch cycle test, owing to the increases in the anode surface area and the number of bacteria attached to anode, the increase in the transient power was more remarkable.

INTRODUCTION

Microbial fuel cell (MFC) is an environment-friendly and sustainable power device, which can generate electricity via oxidation of various organic substrates available in wastewaters or sediments with the help of electro-active bacteria. The anode material that directly or indirectly interacts with bacteria is considered to be an important factor affecting the anode performance and thus the overall power output of an MFC. Numerous efforts have been dedicated to improve the power performance by using modified carbon-based anode materials, and recent years have witness an great enhancement in the maximum power density of MFC, from 0.001-0.01 mW m⁻² in 1999 to 2000-3000 mW m⁻² in 2012.^{1,2} The general principles for the anode modifications include the functionalization of anode surfaces with chemical species and the incorporation of high-surface-area conductive materials. The representative examples of the first aspect were (i) the oxidation of the graphite anodes or carbon felt anodes using acids³⁻⁵ in order to induce oxygen functional groups like quinones that are beneficial to electron transfer, and (ii) the nitrogen functionalization of the carbon cloth anodes using heat ammonia treatment^{6,7} or dimethylaniline⁸ in order to produce protonated amine groups that are conducive to bacteria adhesion. The representative examples of the second aspect were the decoration of the carbon-based anode with

conducting polymers,^{9,10} carbon nanotubes (CNTs),¹¹⁻¹⁴ noble metals,¹⁵⁻¹⁷ and graphene,¹⁸⁻²¹ which led to a remarkable increase in the overall power output.

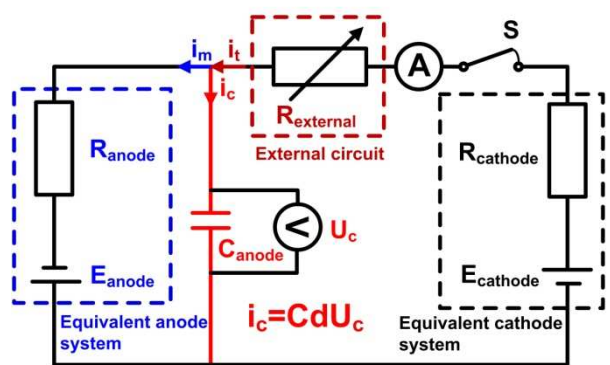
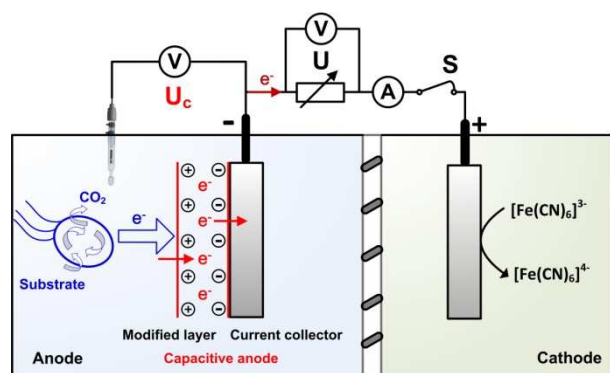
All of the modifying materials favorable to the enhancement in the anode performance have common features including (i) increased electrical conductivity, (ii) increased electrode surface area and (iii) enhanced interactions between the electrode and the electrolyte. It is important to note that these characteristics are indeed desirable for the development of electrode materials in supercapacitors, which store energy via an electrochemical double layer formed at the electrode interface and/or a redox pseudo-capacitive behavior of redox-active species existed on the electrode surface.^{22,23} The modifications of electrode materials in supercapacitors analogous to those related to the anode materials in MFCs are extensively available in the literature. Table 1 lists the representative surface modifications of the electrodes that can be considered for applications in MFCs as well as in supercapacitors. It seems that the modifying materials that are essential for the increase in power performance can also be effective in increasing capacitance. For example, we have previously reported that conductive polypyrrole (PPy) films with the anthraquinone dopants appear to be excellent electrode materials for both MFC⁹ and supercapacitor²⁴ applications. The quinone groups take part in the fast Faradic interactions that are important for mediating electron transfer from the microbes to the anode in MFCs and increasing the specific pseudo-capacitance of

Table 1 List of representative studies concerning surface modifications of electrodes that can be considered for applications in MFCs as well as in supercapacitors

Surface modifications	Methods and material types	End uses
(a) Incorporation of carbon materials		
Carbon nanotube (CNT)	CNT-coated macroporous sponge as an MFC anode	MFCs ¹⁴
	CNT ink dipped into ordinary kitchen sponges	Supercapacitors ²⁵
	Bamboo-like nitrogen-doped CNTs as anode modifying materials	MFCs ¹¹
	Bamboo-shaped N-doped multi-walled CNTs synthesized by chemical vapor deposition method	Supercapacitors ²⁶
	Carbon cloth dipped into the MWCTs ink	MFCs ¹³
	CNT thin films fabricated by electrophoretic deposition	Supercapacitors ²⁷
	CNT-textile composite as an MFC anode	MFCs ²⁸
	Single-walled CNT textile fabricated by “dipping and drying”	Supercapacitors ²⁹
	Multi-walled CNTs modified carbon paper electrode utilizing a layer-by-layer assemble technique	MFCs ³⁰
	Layer-by-layer assembly of all CNT ultrathin films	Supercapacitors ³¹
Graphene	Reduced graphene oxide (RGO) sheets deposited on carbon cloth, stainless steel mesh and carbon paper	MFCs ^{18, 32, 33}
	Homogeneous RGO films pasted on titanium	Supercapacitors ³⁴
	Graphene electrochemically deposited on carbon cloth	MFCs ¹⁹
	RGO films synthesized by electrophoretic deposition	Supercapacitors ³⁵
	Graphene-polyurethane spong composites fabricated by dipping-and-drying process	MFCs ²¹
Graphite particles	Graphene/polyurethane composite film fabricated by simple bonding	Supercapacitors ³⁶
	Roll-pressuring the mixture of graphite particles and polytetrafluoroethylene emulsion	MFCs ³⁷
Mesoporous carbon	Porous graphite particles coated on nickel-foam substrates	Supercapacitors ³⁸
	Mesoporous carbon modified carbon paper as an MFC anode	MFCs ³⁹
Carbon nanofibers	Graphite fiber overlaid with mesoporous carbons by casting	Supercapacitors ⁴⁰
	Activated carbon nanofiber nonwoven as an MFC anode	MFCs ⁴¹
	Electro-spinning poly(acrylonitrile) solutions in dimethylformamide to form carbon nanofiber	Supercapacitors ⁴²
(b) Surface functionalization		
Nitrogen and oxygen functionalization of carbon materials	HNO ₃ -treatment of carbon mesh or activated carbon fiber felt	MFCs ^{4, 43}
	Preoxidation of carbon materials treated with HNO ₃	Supercapacitors ⁴⁴
	Ammonia gas-or dimethylaniline-treatment of carbon cloth	MFCs ^{6, 8}
	Preparation of nitrogen-enriched carbons by ammoxidation or melamine resins treatment	Supercapacitors ^{45, 46}
(c) Incorporation of conductive polymers/metallic oxides		
Conductive polymers	Polypyrrole (PPy) with the anthraquinone-2,6-disulphonic disodium salt (AQDS) coated on the carbon felt anode	MFCs ^{9, 47}
	Electropolymerization of PPys with different anthraquinone groups	Supercapacitors ²⁴
	Coating polyaniline (PANI) nano-fibers on the surface of carbon cloth	MFCs ⁴⁸
	PANI deposited on hollow carbon spheres	Supercapacitors ⁴⁹
Metallic oxides (RuO ₂ /Fe ₃ O ₄ /WO ₃ /TiO ₂)	RuO ₂ coating on the carbon felt electrode via electrodeposition	MFCs ^{17, 47}
	Electrodeposition of RuO ₂ thin films on titanium	Supercapacitors ⁵⁰
	Fe ₃ O ₄ added into the activated carbon with a stainless steel anode	MFCs ⁵¹
	Fe ₃ O ₄ deposited on carbon papers by spray	Supercapacitors ⁵²
	m-WO ₃ /PANI pasted on carbon felt	MFCs ⁵³
	Ordered WO ₃ nanowire arrays on carbon cloth conductive substrates	Supercapacitors ⁵⁴
	Mesoporous nanostructured PANI/TiO ₂ as an MFC anode	MFCs ⁵⁵
	Hydrogenated TiO ₂ obtained by a calcinations of anodized TiO ₂ nanotube arrays in hydrogen atmosphere	Supercapacitors ⁵⁶
(d) Incorporation of hybrid composites		
PPy/CNT	PPy-coated CNT composites as an MFC anode	MFCs ⁵⁷
	PPy/CNT composites on tantalum by electrodeposition	Supercapacitors ⁵⁸
PANI/CNT	PANI/CNTs coated on the nickel foam anode	MFCs ⁵⁹
	PANI/CNTs nanocomposite synthesized through polymerization	Supercapacitors ⁶⁰
PANI/graphene	Decoration of graphene with PANI through in situ polymerization	MFCs ⁶¹⁻⁶³
	Fibrillar PANI doped with graphene oxide sheets synthesized via in situ polymerization	Supercapacitors ⁶⁴
PPy/graphene	One-step electrosynthesis of PPy/graphene oxide composites on the graphite felt electrode	MFCs ⁶⁵
	Graphene oxide/PPy nanocomposites via one-step coelectrodeposition	Supercapacitors ⁶⁶
PPy/carbon black	PPy/carbon black composite coated on carbon paper	MFCs ⁶⁷
	Carbon black/PPy nanocomposites prepared via in situ chemical oxidative polymerization	Supercapacitors ⁶⁸
TiO ₂ /CNT	CNT@TiO ₂ nanohybrids coated on both sides of carbon cloth	MFCs ⁶⁹
	TiO ₂ deposited on CNT by sol-gel process	Supercapacitors ⁷⁰

the electrode in supercapacitors.

However, when these capacitive materials are utilized in the anode, an overestimate of MFC performance may occur due to the contribution of anode charging and discharging to the power measured. For the commonly used polarization techniques such as varying circuit resistance (VCR) or linear sweep voltammetry (LSV), it is difficult to obtain the steady-state anode potentials. Take VCR as an example in which the cell potential is generally recorded when the MFC is continuously run at a fixed resistance over 20 min,⁷¹ but this period of time may still not be sufficient for eliminating the effect of anode discharging when the anode has high capacitance. Therefore, the power measured from these methods is considered to be transient power rather than stationary power. This point can be further illustrated in Fig. 1.



Varying circuit resistance (VCR) method

Fig. 1 (a) Electron flow from microbial oxidation of substrate to the terminal electron acceptor (i.e., hexacyanoferrate) via the capacitive anode and the external circuit; (b) Equivalent circuit of a dual-chamber MFC in which the anode functions as a capacitor that accumulates electrons from bacteria. R_{anode} and $R_{cathode}$ represent the sum of charge-transfer resistance, diffusion resistance and ohmic resistance at the anode and cathode, respectively.

The total current (i_t) passing through the external resistance is considered to be the sum of contribution by two processes, the capacitor current (i_c) resulted from the release of stored electrons in the anode and the microbial current (i_m) originated from cell metabolism, as described by:

$$i_t = i_c + i_m \quad (1)$$

Considering i_c is the differential result of charge (Q_C) released

from the anode as a function of time (t) and Q_C equals to the product of anode capacitance (C) and the change of potential (dU_c) at the anode, we get:

$$i_c = \frac{dQ_c}{dt} = \frac{C \times dU_c}{dt} \quad (2)$$

It is evident that i_c is variable depending on the change of anode potential. If $dU_c > 0$, the contribution of anode discharging can not be neglected and the overall power obtained is the transient power; if $dU_c = 0$, all the contribution comes from microbial process and the overall power is the stationary power.

The aims of this study were thus (i) to compare the transient and stationary power of the MFC equipped with the capacitive anode; and (ii) to explain how the anode capacitance affects the transient and stationary power. To meet these goals, a series of graphite felt anodes modified with polypyrrole/graphene oxide (PPy/GO) composites that exhibit different capacitances were prepared and power performance of MFCs with these anodes was examined.

Materials and methods

Preparation of high-capacitance anode materials

Graphene along with conducting polymer like polypyrrole (PPy) are widely used in rechargeable electrochemical devices such as supercapacitor and lithium battery due to the high electrical conductivity and large surface area of graphene and good reversible redox reactions of PPy.^{66, 72-75} Here, PPy/GO-coated graphite felt electrodes as the anodes were prepared according to the procedures described in our previous work.⁶⁵ The detailed procedures were described in ESI†. The difference in capacitance among the PPy/GO materials was controlled by varying the total charge passed to the working electrode. The freshly prepared PPy/GO-modified graphite felt anodes were then thoroughly rinsed with distilled water and air-dried at room temperature. It should be noted that all the potentials reported throughout this paper were referred to saturated calomel electrode (SCE), if not otherwise stated.

MFC construction, operation and tests

The two-chamber MFC made of Perspex frames was fabricated as described previously¹⁷, consisting of the modified graphite felt anode and a bare graphite felt cathode (3.0 cm × 2.0 cm × 0.5 cm) in each chamber. The two chambers were separated by a cation exchange membrane (Zhejiang Qianqiu Group Co., Ltd. China) with each having an effective volume of 25 mL. The anode chamber was inoculated with *Shewanella oneidensis* MR-1 purchased from ATCC (700550). The anolyte contained the lactate-growth medium including 20 mM lactate and 0.1 M phosphate buffer solution (PBS)-based nutrient solution (pH 8.0) consisting of 5.84 g L⁻¹ NaCl, 0.10 g L⁻¹ KCl, 0.25 g L⁻¹ NH₄Cl, 10 mL of vitamin solution and 10 mL of mineral solution. The cathode chamber was fed with a PBS solution (0.1 M, pH 7.0) containing 50 mM potassium hexacyanoferrate as the electron acceptor. All MFCs were operated at a controlled temperature of 30 °C. A 32-channel voltage collection instrument (AD8223, China) was used to record the cell potential across the external resistance every 5 min.

Polarization and power density curves were obtained by three

different methods (Fig. S1 in ESI†), when the performance of MFC approached steady state after several times of lactate replenishment. For the VCR method, the potential at different resistances (i.e., open-circuit, 2000, 1000, 500, 250, 100, 50 and 25 Ω) with time duration ranging from 5 to 20 min was recorded. For the LSV method, the CHI 660C potentiostat was used to record the polarization curve by running LSV at different scan rates (i.e., 1, 0.5 and 0.2 mV s^{-1}). To obtain the polarization curve, the potentiostat was operated in a two-electrode mode, with the cathode serving as the working electrode, and the anode acting as both the reference and counter electrodes. In addition, the third method, fed-batch cycle test method,⁷⁶ was conducted; in which the maximum sustainable potential over the cycle (that typically sustained for 4 to 12 h depending on the total length of the cycle) was recorded using a single resistor over a complete fed-batch cycle. Each resistance (i.e., open-circuit, 2000, 1000, 500, 250, 100, 50 and 25 Ω) was tested for three consecutive cycles to ensure that the potential response was unchanged upon different cycles. For the above methods, the variations in the anode potential were obtained by inserting a SCE electrode into the anode chamber. The UT-805A desktop multimeter (ShenZhen Uni-Trend Group Limited, China) that connects to a computer was used for recording the cell potential and the anode potential. The capacitance of the inoculated materials was examined through the galvanostatic charge-discharge tests that were performed at a current load of 0.5 mA cm^{-2} within the potential window from -0.6 to 0.3 V. The electrochemical impedance spectra (EIS) measurements of the anode were recorded at the open circuit potential (OCP) and in the frequency range from 10000 to 0.01 Hz with a sinusoidal excitation signal of 10 mV. All these electrochemical tests were carried out in the three-electrode mode using the anode as the working electrode, the cathode as the counter electrode, and a sterilized SCE inserted in the anode chamber as the reference electrode.

Independently repeated experiments with respect to each anode were carried out to test reproducibility. The results shown in the following figures came from a representative experiment if the data obtained from duplicate experiments exhibited negligible difference; otherwise, the average value of duplicate experiments was given, with error bars showing the standard deviations.

Scanning electron microscope (SEM) tests

Surface morphologies of the electrodes were examined using scanning electron microscope (SEM) (S-3700N, Hitachi, Japan). The stabilization of the bacteria attached to the anode was referred to the procedures described elsewhere.^{9, 65} Briefly, the sample (cut from the anode) was first immersed in 3% glutaraldehyde solution for 5h. It was then rinsed with a PBS solution (pH 7.0) three times, followed by dehydration with increasing concentration of ethanol (34%, 50%, 75%, and 95%) for 10 min each and further rinses in isoamyl acetate twice (10 min each time). The sample was dried at CO_2 -critical point for 3 h. Prior to SEM tests, the sample was sputtered with a thin coating layer of gold.

Results and discussion

Transient power density obtained from VCR and LSV

Both LSV and VCR techniques have been widely used for

obtaining polarization data, from which the power curve can be further obtained. The resulting power densities are often recorded under the transient conditions, thus much higher than those sustained at a fixed resistance over long time.⁷⁷ Many previous studies^{76, 78, 79} have concluded that the variations in the measured power densities were attributed to the changes in the anode potentials, which were influenced by the insufficient acclimation time for anode biofilm to adapt to a rapid change of potential for the LSV method, or a new resistance for the VCR method.⁷⁶ However, the anode materials with different capacities to store electrons can also result in the changes in the anode potentials, an important factor which is often ignored.

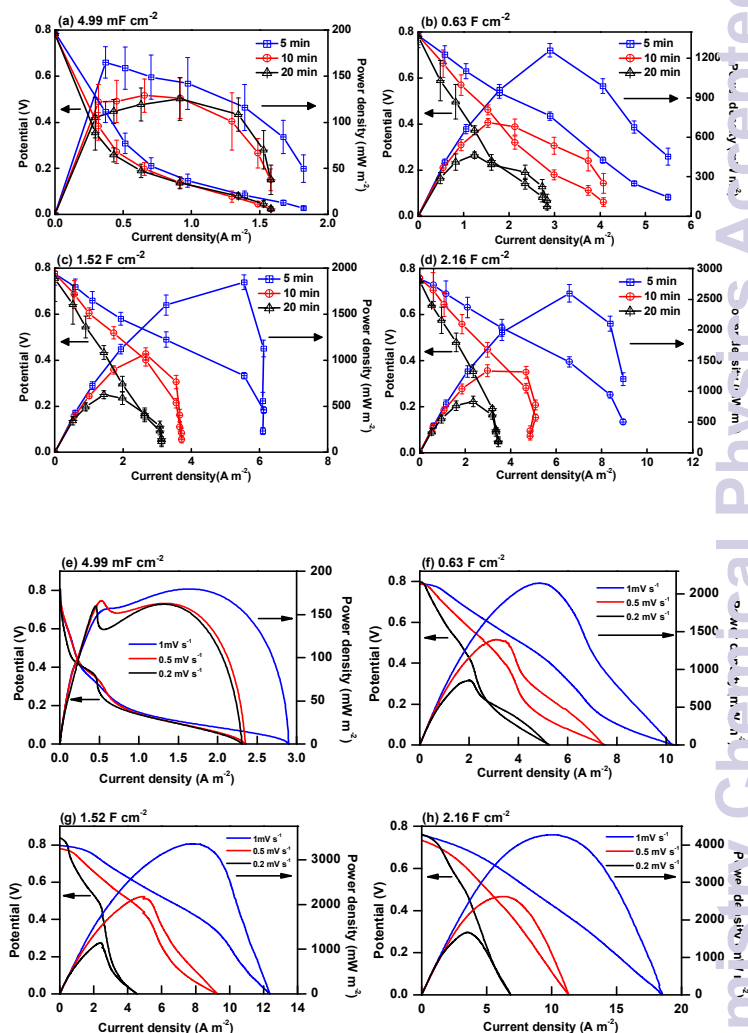


Fig. 2 Polarisation and power density curves of MFCs with different PPy/GO-modified graphite felt anodes obtained from the VCR (a~d) and LSV (e~h).

To identify effects of the anode capacitance on the maximum power density, polarization data were obtained from the LSV and VCR techniques that were run on the MFCs with PPy/GO composites-modified anodes. A series of anode materials were synthesized and their capacitances were determined by the galvanostatic tests (Fig. S2 in ESI†). It should be noted that the capacitances of the inoculated anode materials were recorded because the biofilm enriched on the anode can also show the

ability of storing electrons,^{80, 81} although we have previously shown that the capacitance of the biofilm was one to two orders of magnitude lower than that of the synthesized anode materials.⁴⁷ Fig. 2 clearly shows that the maximum power density obtained from two methods varied considerably, depending on the anode capacitance and the scan rate (LSV) or the time duration at a fixed resistance (VCR). For the unmodified anode with the lowest capacitance, the polarization curves and power density curves obtained from different operations exhibited small variances. Increasing the anode capacitance resulted in remarkable difference; this effect was more pronounced when the scan rate was 1.00 mV s⁻¹ or the time duration was 5 min in comparison to 0.20 mV s⁻¹ or 20 min, respectively. For example, for the MFC with the anode capacitance of 4.99 × 10⁻³ F cm⁻², the maximum power density of recorded at 1.00 mV s⁻¹ was 179.54 mW m⁻², 1.11 times as compared to that (161.94 mW m⁻²) recorded at 0.20 mV s⁻¹. This ratio increased to 2.57 for the MFC with the anode capacitance of 2.16 F cm⁻², as the maximum power density was 4277.48 and 1665.70 mW m⁻², corresponding to 1.00 and 0.20 mV s⁻¹, respectively. All the data in Fig. 2 provided evidence that noticeable transient power was recorded when the commonly used methods was chosen for measuring the power produced in MFCs, particularly in regards to those equipped with high-capacitance anode materials. The changes in the transient power were mainly attributed to the variations in the anode performance, as confirmed by the anode and cathode polarization curves. Clear visible from Fig. S3 in ESI† was the distinct differences in the anode potentials depending on the time duration at a fixed resistance (for the VCR method) or the scan rate (for the LSV method) in comparison to the insignificant differences in the cathode potentials among the MFCs.

Calculations on the contribution of anode capacitance to the maximum power density obtained from VCR or LSV

Calculations were further performed in an attempt to elucidate the contribution of anode capacitance to the maximum power density obtained from VCR and LSV. As illustrated in Fig. 1, when the cell potential (U) was recorded at a fixed resistance (R), the total current (i_t) and the maximum power density (P_t) can be subsequently calculated as Eq. 3 and Eq. 4, respectively.

$$i_t = \frac{U}{R} \quad (3)$$

$$P_t = \frac{U \times i_t}{A} \quad (4)$$

where A is the projected anode surface area. Substituting Eq. 1 into Eq. 4, we get:

$$P_t = \frac{U}{A} i_m + \frac{U}{A} i_c = P_m + P_c \quad (5)$$

where P_m and P_c refers to the part of maximum power density contributed by microbial process and capacitive process, respectively.

To quantify the specific values of P_m and P_c , it is necessary to know the values of i_m and i_c at the time when P_t was obtained. Assuming that i_c exhibits negligible variation at the time interval (Δt) just prior to the measurement of P_t , we get:

$$i_c = \frac{C \times \Delta U_c}{\Delta t} \quad (6)$$

It should be noted that Δt was set at 20 s for the following calculations according to the considerations including that (i) Δt should be kept as small as possible so that i_c is constant; and (ii) the change in the anode potential (ΔU_c) within the time interval is detectable from the multimeter (the detection limit is 0.001 mV). By measuring the values of ΔU and C , and using Eq. 6, we can determine the value of i_c . Note, however, that the value of C varies depending on the charge-discharge current rather than a constant⁸², meaning that C is in turn a function of i_c . Calibration of i_c and C was performed using the iterative method, as depicted by the algorithm in ESI†.

Substituting Eq. 6 into Eq. 1 and rearranging the terms lead to:

$$i_m = i_t - \frac{C \times \Delta U_c}{\Delta t} \quad (7)$$

By knowing the values of P_m and P_c , we can quantitatively assess the contribution of different sources. The percentage of anode discharging and cell metabolism accounted for the total maximum power density is thus introduced:

$$\eta_m = \frac{P_m}{P_t} = \frac{U \times i_m}{P_t} \quad (8)$$

$$\eta_c = \frac{P_c}{P_t} = \frac{U \times i_c}{P_t} \quad (9)$$

Fig. 3 shows that the magnitude of individual contribution was critically affected by the anode capacitance and the time duration at a fixed resistance. When the time duration was 5 min (Fig. 4a), the microbial contribution accounted for the greatest percentage (85.2%), whereas the capacitor contribution was negligible for the MFC equipped with the unmodified anode having a specific capacitance of 4.99 × 10⁻³ F cm⁻². Increasing the capacitance of the PPy/GO-modified anode from 4.99 × 10⁻³ to 0.63 F cm⁻² greatly decreased the percentage of the microbial contribution from 85.2% to 20.0%, and increased the percentage of the capacitor contribution from 14.8% to 80.0%. Further increases in the capacitance resulted in further decreases in the microbial contribution. When the PPy/GO-modified anode had the highest capacitance (2.16 F cm⁻²), the capacitor contribution (87.9%) was much more important than the microbial contribution (less than 12.1%), revealing that the electrons released from the anode was predominantly responsible for the measured power output. The effect of anode capacitance on the capacitor contribution was less pronounced when the time duration was longer (Fig. 3b & 3c). For example, when the anode potential was recorded after 20 min-operation of the MFC at a fixed resistance, the percentage of the capacitor contribution was 0.2%, 31.2%, 59.7% and 82.6%, in relation to the anode capacitance of 4.99 × 10⁻³, 0.63, 1.52, and 2.16 F cm⁻², respectively. This was expected because the increased duration time caused a decrease in the value of ΔU_c , and thus a decrease in i_c (Eq. 9).

Fig. S5 in ESI† illustrates the similar trend related to the data obtained from LSV. It was noticeable that the higher the scan rate or the higher the anode capacitance, the larger the percentage of

the capacitor contribution. These results demonstrate that the increased electron-storage capacity of anode materials is responsible for the enhanced transient power measured by VCR or LSV method. This effect is much more pronounced at the time duration of 5 min in comparison to 20 min, or at the scan rate of 1.00 mV s⁻¹ in comparison of 0.20 mV s⁻¹.

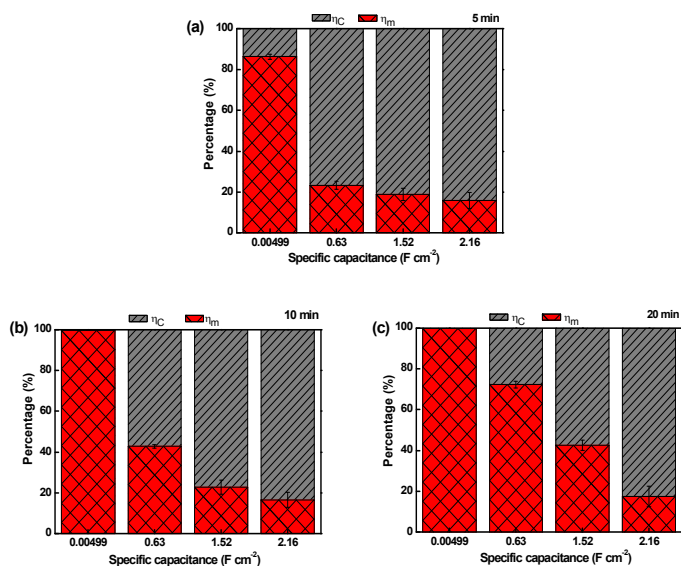


Fig. 3 Variations in the percentage of cell metabolism and anode discharging accounted for the measured maximum power density obtained from VCR.

Stationary power obtained from fed-batch cycle test

As illustrated in Fig. 1, the stationary power can be obtained when there is no change in the anode potential at a fixed resistance. To eliminate the influence of transient current on the measured power, we run the reactor with an external resistance that was fixed throughout one cycle of substrate feeding. Polarization curves were obtained by performing the tests of multiple cycles, each at different fixed resistances.^{71, 76} Fig. 4a shows the stationary data produced in MFCs with different anode capacitances. Clearly visible was that the stationary maximum power densities were much lower than the transient values shown in Fig. 2. Nevertheless, increasing the anode capacitance can significantly increase the stationary power. This is because the increased anode capacitance is directly linked to more active sites provided for mass or charge transfer, which is also reflected by increased anode surface area. The anode and cathode polarization curves (Fig. 4b) further verified that the difference in the anode performance was responsible for different power performance as the anode polarization was highly relied on anode capacitance and the cathode polarization exhibited negligible variations. It was evident from Fig. 5 that the increased surface area allowed increased amounts of bacteria attached to the anode. Many previous studies^{33, 62, 63} have shown that the bio-electricity greatly benefit from the growing number of bacteria adhered. The EIS data (Fig. S6 in ESI†) provided further evidence that the anode with the increased amounts of bacteria resulted in the decrease in the electron transfer resistance, as indicated by the decreased diameter of the semicircle appeared in the middle and low frequency range.

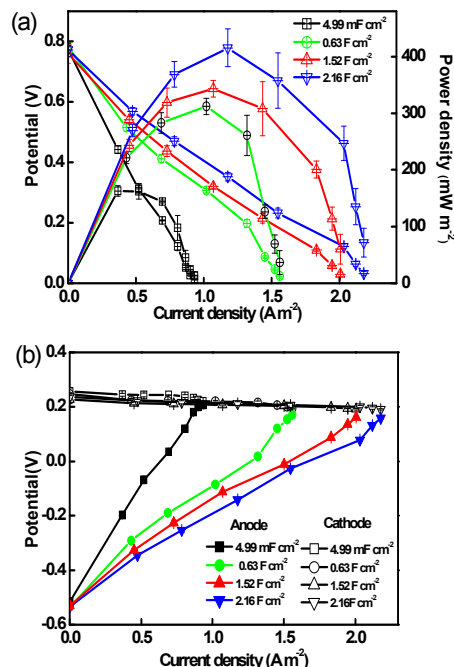


Fig. 4 (a) Power density curves and cell polarization curves, and (b) anode and cathode polarization curves of MFCs with different PPy/GO-modified graphite felt anodes obtained from fed-batch cycle tests.

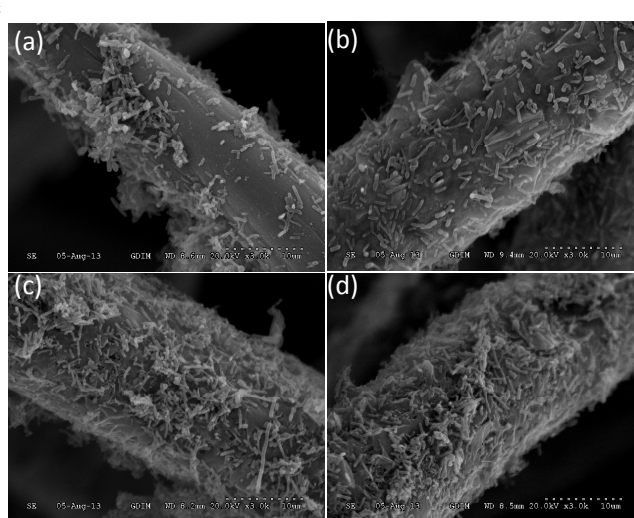


Fig. 5 SEM images of different anodes inoculated with *Shewanella oneidensis* MR-1 (a) unmodified anode (4.99 × 10⁻³ F cm⁻²), (b) PPy/GO-modified anode (0.63 F cm⁻²), (c) PPy/GO-modified anode (1.52 F cm⁻²), and (d) PPy/GO-modified anode (2.16 F cm⁻²).

Conclusions

Here we demonstrated that the discharge of bioelectrons stored in the high-capacitance anode was a dominant contributor to the measured maximum power density, especially when the time duration at a fixed resistance was not sufficiently long (for the VCR method) or the scan rate was not sufficiently low (for the LSV method). Our results showed that the MFC power performance was overestimated when the anode discharging

constituted a significant part of the total current passed through the external circuit. This means that anode modification with capacitive materials led to a remarkable increase in the transient power. Nevertheless, the anode materials with high capacitance can also give rise to the increased stationary power, because it enabled increased electrical conductivity, increased anode surface area and an increase in the number of bacteria attached to anode. Therefore, the anode capacitance is still an important consideration for the design of MFC anodes. Furthermore, the MFC anode incorporating pseudo-capacitive materials can function as a biocapacitor⁴⁷ that shows potential for storing energy from waste organic matter and releasing in a short time of high power to the electronic device.

Acknowledgements

We gratefully acknowledge financial support from the National Natural Science Foundation of China (No. 21177042, No. 21037001), the Program for New Century Excellent Talents in University (no. NCET-12-0198) and the Fundamental Research Funds for the Central Universities, SCUT (No. 2014ZG0014).

Author address

^a The Key Lab of Pollution Control and Ecosystem Restoration in Industry Clusters, Ministry of Education, College of Environment and Energy, South China University of Technology, Guangzhou 510006, PR China. Fax: 86-20-39380588; Tel: 86-20-39380502; E-mail: chfeng@scut.edu.cn

[†] Electronic Supplementary Information (ESI) available: [details of any supplementary information available should be included here]. See DOI: 10.1039/b000000x/

References

- D. Pant, A. Singh, G. Van Bogaert, S. I. Olsen, P. S. Nigam, L. Diels and K. Vanbroekhoven, *RSC Advances*, 2012, **2**, 1248-1263.
- B. E. Logan and K. Rabaey, *Science*, 2012, **337**, 686-690.
- K. Scott, G. Rambu, K. Katuri, K. Prasad and I. Head, *Process Safety and Environmental Protection*, 2007, **85**, 481-488.
- N. Zhu, X. Chen, T. Zhang, P. Wu, P. Li and J. Wu, *Bioresource Technology*, 2011, **102**, 422-426.
- Y. Feng, Q. Yang, X. Wang and B. E. Logan, *Journal of Power Sources*, 2010, **195**, 1841-1844.
- S. Cheng and B. E. Logan, *Electrochemistry Communications*, 2007, **9**, 492-496.
- X. Wang, S. Cheng, Y. Feng, M. D. Merrill, T. Saito and B. E. Logan, *Environmental Science and Technology*, 2009, **43**, 6870-6874.
- T. Saito, M. Mehanna, X. Wang, R. D. Cusick, Y. Feng, M. A. Hickner and B. E. Logan, *Bioresource Technology*, 2011, **102**, 395-398.
- C. Feng, L. Ma, F. Li, H. Mai, X. Lang and S. Fan, *Biosensors and Bioelectronics*, 2010, **25**, 1516-1520.
- C. Li, L. Zhang, L. Ding, H. Ren and H. Cui, *Biosensors and Bioelectronics*, 2011, **26**, 4169-4176.
- S. Ci, Z. Wen, J. Chen and Z. He, *Electrochemistry Communications*, 2012, **14**, 71-74.
- P. Liang, H. Wang, X. Xia, X. Huang, Y. Mo, X. Cao and M. Fan, *Biosensors and Bioelectronics*, 2011, **26**, 3000-3004.
- H.-Y. Tsai, C.-C. Wu, C.-Y. Lee and E. P. Shih, *Journal of Power Sources*, 2009, **194**, 199-205.
- X. Xie, M. Ye, L. Hu, N. Liu, J. R. McDonough, W. Chen, H. Alshareef, C. S. Criddle and Y. Cui, *Energy and Environmental Science*, 2012, **5**, 5265-5270.
- Y. Fan, S. Xu, R. Schaller, J. Jiao, F. Chaplen and H. Liu, *Biosensors and Bioelectronics*, 2011, **26**, 1908-1912.
- M. Sun, F. Zhang, Z.-H. Tong, G.-P. Sheng, Y.-Z. Chen, Y. Zhao, Y.-P. Chen, S.-Y. Zhou, G. Liu and Y.-C. Tian, *Biosensors and Bioelectronics*, 2010, **26**, 338-343.
- Z. Lv, D. Xie, X. Yue, C. Feng and C. Wei, *Journal of Power Sources*, 2012, **210**, 26-31.
- L. Xiao, J. Damien, J. Luo, H. D. Jang, J. Huang and Z. He, *Journal of Power Sources*, 2012, **208**, 187-192.
- J. Liu, Y. Qiao, C. X. Guo, S. Lim, H. Song and C. M. Li, *Bioresource Technology*, 2012, **114**, 275-280.
- Y.-X. Huang, X.-W. Liu, J.-F. Xie, G.-P. Sheng, G.-Y. Wang, Y.-Y. Zhang, A.-W. Xu and H.-Q. Yu, *Chemical Communications*, 2011, **47**, 5795-5797.
- X. Xie, G. Yu, N. Liu, Z. Bao, C. S. Criddle and Y. Cui, *Energy and Environmental Science*, 2012, **5**, 6862-6866.
- P. Simon and Y. Gogotsi, *Nature Materials*, 2008, **7**, 845-854.
- M. Zhi, C. Xiang, J. Li, M. Li and N. Wu, *Nanoscale*, 2013, **5**, 72-88.
- X. Lang, Q. Wan, C. Feng, X. Yue, W. Xu, J. Li and S. Fan, *Synthetic Metals*, 2010, **160**, 1800-1804.
- W. Chen, R. Rakhi and H. Alshareef, *Journal of Materials Chemistry*, 2012, **22**, 14394-14402.
- Y. Zhang, C. Liu, B. Wen, X. Song and T. Li, *Materials Letters*, 2011, **65**, 49-52.
- C. Du and N. Pan, *Nanotechnology*, 2006, **17**, 5314.
- X. Xie, L. Hu, M. Pasta, G. F. Wells, D. Kong, C. S. Criddle and Y. Cui, *Nano Letters*, 2010, **11**, 291-296.
- L. Hu, M. Pasta, F. L. Mantia, L. Cui, S. Jeong, H. D. Deshazer, J. W. Choi, S. M. Han and Y. Cui, *Nano Letters*, 2010, **10**, 708-714.
- J.-J. Sun, H.-Z. Zhao, Q.-Z. Yang, J. Song and A. Xue, *Electrochimica Acta*, 2010, **55**, 3041-3047.
- S. W. Lee, B.-S. Kim, S. Chen, Y. Shao-Horn and P. T. Hammond, *Journal of the American Chemical Society*, 2008, **131**, 671-679.
- Y. Zhang, G. Mo, X. Li, W. Zhang, J. Zhang, J. Ye, X. Huang and C. Yu, *Journal of Power Sources*, 2011, **196**, 5402-5407.
- J.-R. Zhang, C. Zhao, Y. Wang, F. Shi and J.-J. Zhu, *Chemical Communication*, 2013, **49**, 6668-6670.
- Y. Chen, X. Zhang, D. Zhang, P. Yu and Y. Ma, *Carbon*, 2011, **49**, 573-580.
- T. Lu, L. Pan, H. Li, C. Nie, M. Zhu and Z. Sun, *Journal of Electroanalytical Chemistry*, 2011, **661**, 270-273.
- Z. Tai, X. Yan and Q. Xue, *Journal of Power Sources*, 2012, **213**, 350-357.
- T. Zhang, Y. Zeng, S. Chen, X. Ai and H. Yang, *Electrochemistry Communications*, 2007, **9**, 349-353.
- Z. Chen, J. Wen, C. Yan, L. Rice, H. Sohn, M. Shen, M. Cai, B. Dunn and Y. Lu, *Advanced Energy Materials*, 2011, **1**, 551-556.

39. Y. Zhang, J. Sun, B. Hou and Y. Hu, *Journal of Power Sources*, 2011, **196**, 7458-7464.
40. F. Luffrano and P. Staiti, *International Journal of Electrochemical Science*, 2010, **5**, 903-916.
41. S. S. Manickam, U. Karra, L. Huang, N.-N. Bui, B. Li and J. R. McCutcheon, *Carbon*, 2013, **53**, 19-28.
42. C. Kim and K. Yang, *Applied Physics Letters*, 2003, **83**, 1216-1218.
43. M. Zhou, M. Chi, H. Wang and T. Jin, *Biochemical Engineering Journal*, 2012, **60**, 151-155.
44. Z. Gu, J. Hong, X. Wang and J. Polin, *Journal of Power Sources*, 2013, **236**, 285-292.
45. K. Jurewicz, K. Babel, A. Ziólkowski and H. Wachowska, *Electrochimica Acta*, 2003, **48**, 1491-1498.
46. D. Hulicova, J. Yamashita, Y. Soneda, H. Hatori and M. Kodama, *Chemistry of Materials*, 2005, **17**, 1241-1247.
47. Z. Lv, D. Xie, F. Li, Y. Hu, C. Wei and C. Feng, *Journal of Power Sources*, 2014, **246**, 642-649.
48. B. Lai, X. Tang, H. Li, Z. Du, X. Liu and Q. Zhang, *Biosensors and Bioelectronics*, 2011, **28**, 373-377.
49. Z. Lei, Z. Chen and X. Zhao, *The Journal of Physical Chemistry C*, 2010, **114**, 19867-19874.
50. B.-O. Park, C. Lokhande, H.-S. Park, K.-D. Jung and O.-S. Joo, *Journal of Materials Science*, 2004, **39**, 4313-4317.
51. X. Peng, H. Yu, X. Wang, Q. Zhou, S. Zhang, L. Geng, J. Sun and Z. Cai, *Bioresource Technology*, 2012, **121**, 450-453.
52. W. Shi, J. Zhu, D. H. Sim, Y. Y. Tay, Z. Lu, X. Zhang, Y. Sharma, M. Srinivasan, H. Zhang and H. H. Hng, *Journal of Materials Chemistry*, 2011, **21**, 3422-3427.
53. Y. Wang, B. Li, L. Zeng, D. Cui, X. Xiang and W. Li, *Biosensors and Bioelectronics*, 2013, **41**, 582-588.
54. L. Gao, X. Wang, Z. Xie, W. Song, L. Wang, X. Wu, F. Qu, D. Chen and G. Shen, *Journal of Materials Chemistry A*, 2013, **1**, 7167-7173.
55. Y. Qiao, S.-J. Bao, C. M. Li, X.-Q. Cui, Z.-S. Lu and J. Guo, *ACS Nano*, 2008, **2**, 113-119.
56. X. Lu, G. Wang, T. Zhai, M. Yu, J. Gan, Y. Tong and Y. Li, *Nano Letters*, 2012, **12**, 1690-1696.
57. Y. Zou, C. Xiang, L. Yang, L.-X. Sun, F. Xu and Z. Cao, *International Journal of Hydrogen Energy*, 2008, **33**, 4856-4862.
58. J. Wang, Y. Xu, X. Chen and X. Sun, *Composites science and Technology*, 2007, **67**, 2981-2985.
59. Y. Qiao, C. M. Li, S.-J. Bao and Q.-L. Bao, *Journal of Power Sources*, 2007, **170**, 79-84.
60. E. Frackowiak, V. Khomenko, K. Jurewicz, K. Lota and F. Beguin, *Journal of Power Sources*, 2006, **153**, 413-418.
61. J. Hou, Z. Liu and P. Zhang, *Journal of Power Sources*, 2013, **224**, 139-144.
62. Y.-C. Yong, X.-C. Dong, M. B. Chan-Park, H. Song and P. Chen, *ACS Nano*, 2012, **6**, 2394-2400.
63. C. Zhao, P. Gai, C. Liu, X. Wang, H. Xu, J. Zhang and J.-J. Zhu, *Journal of Materials Chemistry A*, 2013, **1**, 12587-12594.
64. H. Wang, Q. Hao, X. Yang, L. Lu and X. Wang, *Electrochemistry Communications*, 2009, **11**, 1158-1161.
65. Z. Lv, Y. Chen, H. Wei, F. Li, Y. Hu, C. Wei and C. Feng, *Electrochimica Acta*, 2013, **111**, 366-373.
66. C. Zhu, J. Zhai, D. Wen and S. Dong, *Journal of Materials Chemistry*, 2012, **22**, 6300-6306.
67. Y. Yuan and S. Kim, *Bulletin of The Korean Chemical Society*, 2008, **29**, 1344-1348.
68. C. Yang, P. Liu and T. Wang, *ACS Applied Materials and Interfaces*, 2011, **3**, 1109-1114.
69. Z. Wen, S. Ci, S. Mao, S. Cui, G. Lu, K. Yu, S. Luo, Z. He and J. Chen, *Journal of Power Sources*, 2013, **234**, 100-106.
70. H.-I. Kim, H.-J. Kim, M. Morita and S.-G. Park, *Bulletin of the Korean Chemical Society*, 2010, **31**, 423-428.
71. B. E. Logan, *ChemSusChem*, 2012, **5**, 988-994.
72. Q. Qu, Y. Zhu, X. Gao and Y. Wu, *Advanced Energy Materials*, 2012, **2**, 950-955.
73. W. Tang, L. Liu, Y. Zhu, H. Sun, Y. Wu and K. Zhu, *Energy and Environmental Science*, 2012, **5**, 6909-6913.
74. X.-T. Chen, K.-X. Wang, Y.-B. Zhai, H.-J. Zhang, X.-Y. Wu, X. Wei and J.-S. Chen, *Dalton Transactions*, 2014, **43**, 3137-3143.
75. Y. Shi, J.-Z. Wang, S.-L. Chou, D. Wexler, H.-J. Li, K. Ozawa, H.-K. Liu and Y.-P. Wu, *Nano Letters*, 2013, **13**, 4715-4720.
76. V. J. Watson and B. E. Logan, *Electrochemistry Communications*, 2011, **13**, 54-56.
77. S. B. Velasquez - Orta, T. P. Curtis and B. E. Logan, *Biotechnology and Bioengineering*, 2009, **103**, 1068-1076.
78. Y. Hong, D. F. Call, C. M. Werner and B. E. Logan, *Biosensors and Bioelectronics*, 2011, **28**, 71-76.
79. X. Zhu, J. C. Tokash, Y. Hong and B. E. Logan, *Bioelectrochemistry*, 2012, **90**, 30-35.
80. N. S. Malvankar, T. Mester, M. T. Tuominen and D. R. Lovley, *ChemPhysChem*, 2012, **13**, 463-468.
81. X. Peng, H. Yu, H. Yu and X. Wang, *Bioresource Technology*, 2013, **138**, 353-358.
82. X. Wang, Y. Zhang, C. Zhi, X. Wang, D. Tang, Y. Xu, Q. Weng, X. Jiang, M. Mitome and D. Golberg, *Nature Communications*, 2013, **4**, 2905.